# Tunability of silicon clathrate film properties by controlled guest-occupation of their cages

Romain Vollondat, Daniel Stoeffler, Daniele Preziosi, Stéphane Roques, Abdelilah Slaoui, Thomas Fix

# Tunability of Silicon Clathrates films properties by controlled guest-occupation of their cages

*Romain Vollondat*[*1], *Daniel Stoeffler*[2], *Daniele Preziosi*[2], *Stéphane Roques*[1], *Abdelilah Slaoui*[1], *Thomas Fix*[1]

[1] Laboratoire des Sciences de l'Ingénieur, de l'Informatique et de l'Imagerie (ICube), CNRS and University of Strasbourg, 23 rue du Loess, 67037 Strasbourg, France

[2] Institut de Physique et Chimie des Matériaux de Strasbourg (IPCMS), UMR7504 CNRS and University of Strasbourg, 23 rue du Loess, 67034 Strasbourg, France

**Abstract**

Type I and Type II Silicon Clathrates are guest-host structure made of silicon polyhedral cages large enough to contain atoms which can be either inserted or evacuated with only a slight volume change of the structure. This feature is of interest not only for batteries or storage applications but also for tuning the properties of the Silicon Clathrates films. The thermal decomposition process can be tuned to obtain $Na_8Si_{46}$ and $Na_{2<x<10}Si_{136}$ Silicon Clathrates films on intrinsic and p-type c-Si (001) wafer. Here, from a unique synthesized $Na_xSi_{136}$ film, a range of resistivity of minimum four order of magnitude is possible by using post-synthesis treatments, switching from metallic to semiconductor behavior as the Na content is lowered. Extended exposition to sodium vapor allows to obtain fully occupied $Na_{24}Si_{136}$ metallic films and annealing under iodine vapor is a way to reach the guest-free $Si_{136}$, a semiconducting metastable form of silicon with a 1.9 eV direct bandgap. Electrical measurements and resistance versus temperature measurements of the Silicon Clathrates films further discriminate the behavior of the various materials as the Na concentration is changing, additionally shouldered by DFT calculations for various guest occupations, further motivating the urge of innovative pathway toward true guest-free Type I and Type II Silicon Clathrates.

*Corresponding author: romain.vollondat@etu.unistra.fr (R. Vollondat, Ph.D. candidate)

## I. Introduction

Clathrates[1] are crystallographic guest-host structures in which the framework is made of a chemical species forming polyhedral cages that can enclose guest of other species. Silicon Clathrates are a subset of this family and as their name implies their framework is made of Silicon atoms which are covalently linked with each other by $sp^3$ bondings. The cavities formed by this framework are large enough to host alkali metals further stabilizing the structure. Silicon Clathrates are themselves divided from binary[2] to quaternary[3] structures as various species of guest atoms can occupy simultaneously the structure. Thus, Silicon Clathrates encompass a wide range of materials with properties varying with the nature of the guest species alluring in various field from thermoelectricity[4,5], superconductivity[6] to photovoltaics[7], batteries[8] and hydrogen storage[9].

Among all those materials, the first inorganic Clathrates synthesized were the binary silicon clathrates of Type I (SiCL-I) $Na_8Si_{46}$ and Type II (SiCL-II)[10] $Na_xSi_{136}$. Both crystal structures are depicted on Figure S1 of the Supplemental Material for easier visualization. The SiCL-I structure crystalizes in a simple cubic system of the $Pm\bar{3}n$ (#223) space group. One unit cell of this structure is made of 8 cages of two kinds: two are relatively small cages denoted $Si_{20}$ exhibiting twelve pentagonal faces, while the remaining six are slightly larger $Si_{24}$ cages made of twelve pentagonal and two hexagonal faces. Each of these cages are filled by exactly one Na atoms corresponding to the $Na_8Si_{46}$ formula. The Type II structure is crystalizing in a face centered cubic lattice of the $Fd\bar{3}m$ (#227) space group. This structure is made of twenty-four cages, of which sixteen are similar to type I, *i.e.* small $Si_{20}$, while the remaining are "large" $Si_{28}$ cages exhibiting twelve pentagonal faces and four hexagonal faces. In contrast to most type of Silicon Clathrates, the Type II structures is characterized by not only its unique ability to be partially filled with guest atoms but also to be able to let guest species in[11] and out[12,13] of structures under certain conditions. This flexibility allows wide range of structures, almost fully empty, as previously demonstrated for the type II germanium clathrates[14], or fully filled, characterized by the usual formula $Na_{0<x<24}Si_{136}$. In the latter case, dimerization of Na in the large cages has been demonstrated under high-pressure high-temperature conditions leading at even higher occupation levels[15].

The occupation of the cages of these structures is known to have striking impact on their structural and optoelectronic properties[16]. In particular, the SICL-II show different behaviors depending upon the cage occupation level. For guest-free or low occupation cases, this material is behaving like a semiconductor with a direct bandgap around 1.9 eV[17] that is beneficial when compared to the indirect 1.1 eV bandgap of "usual" diamond silicon and thus attractive for photovoltaic applications. On the other side, for occupations higher than $x$ = 8, the material turns into a metal similar to its SiCL-I $Na_8Si_{46}$ counterpart. To obtain materials usable for optoelectronic applications, the thermal decomposition pathway[18] used previously for powder or monocrystalline samples has been derived to obtain films of Silicon Clathrates[19,20]. Although better control over the quality and thickness of Silicon Clathrates layer using various processes is still being largely investigated[21–23], a pathway to obtain a control over the cages occupation, in order to grant a tunability of the films' properties is still of importance. Here, we report for the first time the impact of the thermal decomposition parameters on the occupation of the Si-CL films, and we will discuss how our approach to evacuate or intercalate Na atoms in the cages of the structures have a large impact on the properties of the Silicon Clathrates films.

**II. Experimental section**

The two step-process of thermal decomposition used for the synthesis of the Silicon Clathrates films is identical to the one reported in the previous study of the group and in the literature[19,24]. A Na slice is obtained from a Na ingot (99.8% purity, Alfa Aesar, CAS #7440-23-5) and immediately transferred in a hermetic cyclohexane (99+% purity, Alfa Aesar, CAS #110-82-7) filled container to limit the oxidation of the Na. The two chemicals are managed under safety precautions. A Silicon wafer (c-Si (001)) is sliced into rectangular shape of 54 x 37 mm with a thickness of 525 ± 25 µm and washed with a 10 % vol HF solution. The wafers are mainly p-type with resistivity of 1-5 Ω·cm but intrinsic wafers with resistivity over 10 kΩ·cm when electrical measurements of the films are required. Quickly after, the Na slice is placed into an Inconel boat (54 x 18 x 13.3 $mm^3$, ANALAB, ref. AR9001) which is then promptly covered with the sliced silicon wafer. This system is then placed in a stainless-steel tube kept under a 1.5 bar flush of Argon along with a tantalum wire to absorb any trace of oxygen. The tube is placed in a tubular furnace and heated at temperature of either 630°C or 600°C, to obtain

SiCL-I or SiCL-II respectively, using a ramp of 5°C/min and a dwell time between 13 h and 19 h. Once done, the tube is let to reach room temperature naturally and flushed with Argon anew. The Silicon wafer with the synthesized $Na_4Si_4$ zintl phase is exited out of the stainless-steel tube and quickly put in quartz tube to be heated in a dynamic vacuum of maximum $4.5x10^{-5}$ Pa to prevent prolonged any exposure to ambient humidity with the $Na_4Si_4$. When the desired vacuum is reached, the quartz tube is enclosed in a furnace and heated at 400°C with a ramp of 10°C/min for a duration between 1 to 25 h and let to cool down naturally. The obtained sample is washed with ethanol then deionized water to remove any excess Na which is identifiable by the bubbling coming from the surface of the film. The film is then blow-dried and ready for further characterizations or post-treatments.

The process to reduce the amount of Na in the SiCL-II films has been inspired by the one reported by Ammar *et al.*[13]. Instead of using a sealed glass tube heated in an electrical furnace, we recycled the heating and pumping units of a BET instrument to reach a primary vacuum in a test tube previously filled with samples and iodine (99+%, AnalaR NORMAPUR, CAS #7553-56-2) in excess. Once the targeted vacuum is reached, the test tube is sealed, and the pumping system is turned off. Then the test tube is slowly heated to a temperature of 300°C for a 10 h duration and naturally let to cool down. Purple iodine vapor inside and crystallization of iodine on the inner wall of the test tube is witnessed. The experimental setup is shown in Figure S2. The sample is gathered and cleaned with acetonitrile then deionized water and blow-dried. Samples submitted to this treatment show no detection of Iodine under EDS.

X-ray diffraction (XRD) is performed with a Bruker D8 DISCOVER with a Cu $K_{\alpha 1}$ wavelength of 0.154059 nm. Lattice parameters, atomic positions and displacements along with the Na occupation of the synthesized materials were estimated using Jana2006[25] software by performing LeBail and Rietveld refinement on the XRD data taking as reference previously reported structures for SiCL-I[15] and SiCL-II[26]. Energy Dispersive X-ray Spectroscopy (EDS) measurement were performed on the samples using a JEOL JSM-IT200 scanning electron microscope equipped with a DrySD SSD detector with a resolution of 130 eV or less. The conductivity measurements were performed using Hall effect technique using a ECOPIA HMS-5000 system in the Van der Pauw configuration. Contact with the surface of the samples was performed directly on each corner using gold plated spring needles of a diameter of around 100 µm.

Electric conductivity, in the planar orientation, as well as the nature, the mobility and the density of the carriers were determined. Raman spectroscopy and Photoluminescence (PL) are measured at 293 K using a JOBIN YVON LabRam Aramis apparatus with a 532 nm laser. For each sample, measurements were performed using a 532 nm laser at 1.1 mW using a 2400 $g.mm^{-1}$ grating with a 50 µm slit on five different locations of the film with a total exposition time of 4.5 min per spot. The intensity of the laser is kept at 1.1 mW to prevent the degradation of the SiCL into Si at 11 mW[24]. Transport measurements were performed by using a Physical Properties Measurement System DynaCool system of Quantum Desing in a four-point configuration with Ag-stripe electrodes.

**III. Band structure calculations**

Band structure calculations were performed using the Vienna Ab initio Simulation Package (VASP5.4)[27,28] allowing to determine accurately the electronic structure of the considered system. It uses so-called Augmented Plane Waves and is based on the Projector Augmented Wave (PAW)[29] method using pseudopotentials to determine the wave function outside the augmentation region. For such large cells, all calculations are performed with the GGA functional[30], a cut-off energy of 600 eV and a k-points sampling of 8x8x8 or 6x6x6 depending on the symmetry of the Brillouin Zone. After full relaxation of the lattice parameters and the internal structural position for all atoms, the total density of states TDOS and the band structure E(k) were obtained. For a given $Na_xSi_{136}$ system, a symmetry analysis allowed to identify the equivalent cells and to investigate only one cell per group. For example, for $x = 4$ the 70 possible cells reduce to 4 groups having 2, 12, 24 and 32 equivalent elements. The TDOS is obtained by a weighted average over individual TDOS with a unique Fermi level set as the energy origin.

**IV. Results and discussion**

The attention of this study is put on the Na guest atoms enclosed in the synthesized Silicon Clathrates of SiCL-I and SiCL-II films. Let alone the precursor formation step which mainly impacts the type of Silicon Clathrates structures in presence[24], the first

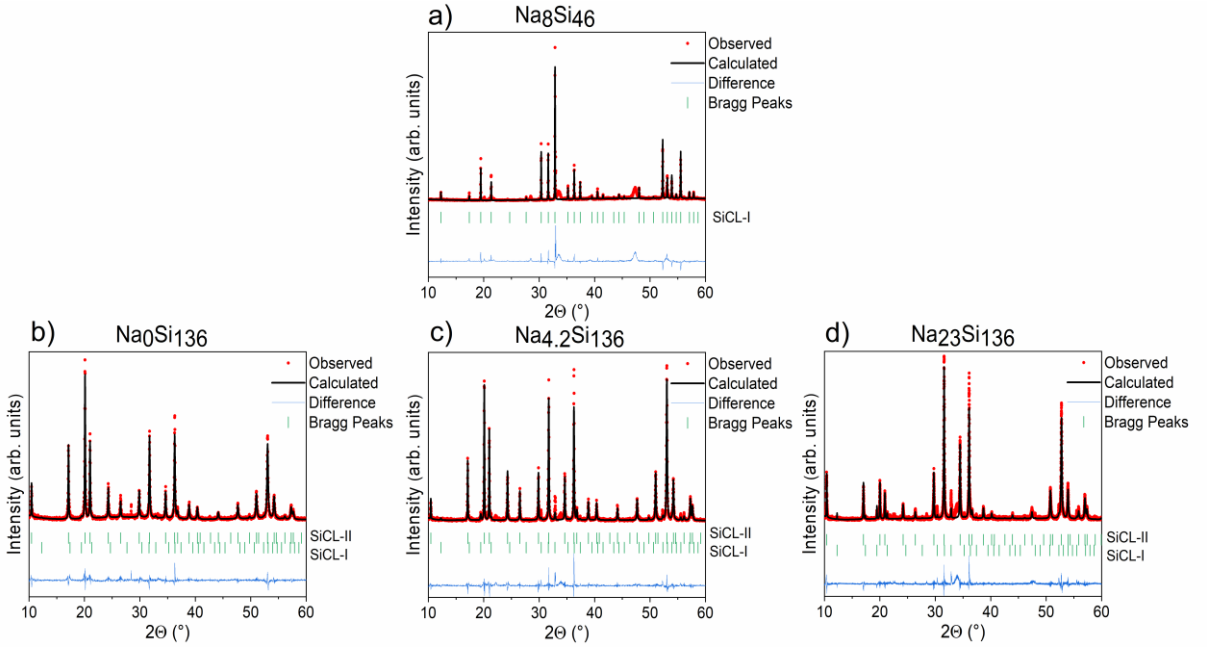


*FIG. 1. XRD diffractogram fitted using Rietveld Refinement for a) SiCL-I and b) SiCL-II with various Na occupations.*

experimental stage with a major impact of the occupation of Na in the structure is the annealing under vacuum step. While the rate of heating has been demonstrated to affect the quality of the film obtained, its duration is the main factor influencing the occupation of the cages. For SiCL-I films, even for extended annealing under vacuum, there are no variations of the X-ray diffractogram peaks profile, visible in Figure 1a, implying that there is no Na removal from the silicon cages of the structure. This inability for the $Na_8Si_{46}$ phase to exhibit cages without guest atoms sustaining them through the thermal decomposition process is an indicator of the low stability of the $Si_{46}$ framework which has only been yet attained in small quantities using Hoffman redox reaction[31]. Considering SiCL-II Silicon Clathrate films this time, when comparing X-ray diffractogram of the samples obtained for various annealing under vacuum duration, large discrepancies are identifiable by the global profile of peaks intensities. As the synthesized films are polycrystalline and that no epitaxial growth has been observed for Type-II SiCL c-Si (001) wafer, these variations of the relative intensities of the peaks are an indicator of the number of Na guest atoms occupying the cages of the structure. To give a better visualization of this assessment, calculated diffraction pattern using the software VESTA[32] at a wavelength of 1.54059 Å for the $Na_xSi_{136}$ structure where the guest occupation has been changed from guest-free (x = 0) to fully occupied (x = 24) by gradual steps are available in Figure S3. For these diffraction patterns, the preferential filling of the large $Si_{28}$ cages over the smaller $Si_{20}$ ones is

taken into account. Roughly speaking the overall profile of the diffraction pattern of SiCL-II can help differentiate between occupation below and above $x = 8$ as visible in Figure 1b,c,d and by comparing with Figure S3. The SiCL-II films usually contains minor SiCL-I for phase fraction from 0 to 2 %.

Additionally, to obtain precise determination of the Na occupation, the software Jana2006 is used to perform LeBail profile refinement followed by a Rietveld refinement of the X-ray diffractogram of the films. The results of these refinements are available in Table SI and indicate a rise in efficiency of the Na atoms exiting mechanism from the SiCL-II as the duration of the annealing under vacuum is extended. A variation of time in this step from 2 to 25 hours can lead to structure with chemical formula

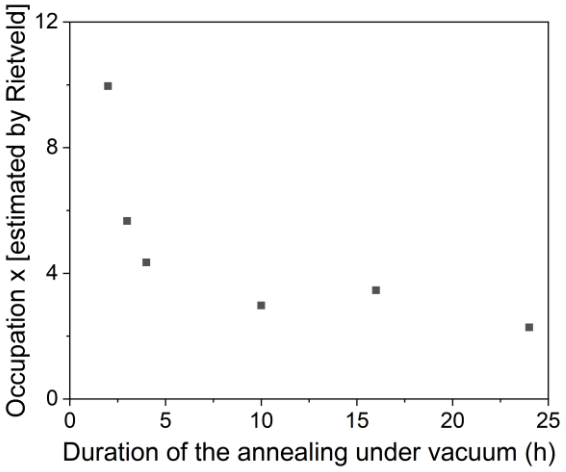


*FIG. 2. Sodium occupation of the SiCL-II structure depending on the duration of the duration of the thermal decomposition of the Zintl phase*

ranging from $Na_9Si136$ to $Na_2Si_{136}$ as visible in Figure 2. When varying only parameters of the synthesis route, no films with consequent filling of the $Si_{20}$ cages nor guest-free films were obtained. The refinements of the lattice parameters along with the atomic positions of the SiCL-II structure show no major change in those values for the studied range of Na concentration.

In order to reach an effective filling of the sixteen small $Si_{20}$ cages, we adapted a method used to intercalate Na atoms in SiCL-II powders[11] for the films studied here. To do so, a similar process than the one performed for the first annealing of the thermal decomposition is used, with the difference that the silicon wafer is replaced by a sapphire wafer on which the SiCL-II films cut into square of around 1.5 x 1.5 $cm^2$ are stick using silver paste. Then the usual method is executed except that the temperature

is lowered to temperature between 320 and 380°C to prevent the degradation of the Silicon clathrates, the mass of the Na slice is of 0.4 g and the reaction time is extended to 50 h. The reaction was performed at three different temperatures. The lowest is 320°C for which no Na addition is witness by XRD nor EDS even though bubbling was observed when washing the samples. The temperature was then boost up to 350°C which allow to rise the Na occupation from $x$ = 4.3 to 6.8 indicating a filling of the remaining empty $Si_{28}$ cages. In order to establish if this result is the real equilibrium of the reaction at 350°C or only due to its slow kinetic, the same sample was resubmitted to the same treatment. This repetition led to the successful filling of the large cages with also some Na atoms taking place in the small cages. A third cycle was performed in order to assess if the temperature was sufficient to fill the small cages but proved inefficient. An annealing at 380°C was then performed and led this time to the filling of almost all the cages of the structure resulting in formula $Na_{23.1}Si_{136}$. All the refined parameters of these samples are available in Table SII. EDS analysis made on the two samples, reported in Figure S4, are in agreement with the refined values of occupation of the samples submitted to Na addition. The lattice parameters refined indicate this time a significant expansion of the structure, which remained almost the same for $x$ between 2.3 to 10 at around 14.63 Å to reach 14.71 Å for $x$ = 23.1. This is consistent with the evolution of the lattice parameter along with the occupation established by Beekman *et al.*[33]. The sudden increase of the Na content of the structure as the temperature is increased successively from 350°C to 380°C underlines that the energy barrier required in order to allow the cages filling seems lower for the $Si_{28}$ polyhedron, which are filled at lower temperature, compared the $Si_{20}$ ones. This is supposedly due to the increasing presence of point defect[12] with the temperature, facilitating the migration of the Na guest throughout the various faces of the cages.

As previously reported[13], annealing under iodine vapour is a reaction which enables the evacuation of the Na atoms out of the SiCL-II cages by the favourable reaction of Iodine with Na to form sodium iodide (NaI). The operation method is adapted from the literature as described in the experimental section. Once washed, one sample was collected while another one was submitted to two more cycles. From a starting film with $x$ = 4.2, the EDS analysis, available in Figure S5, indicates a drop to $x$ = 1.1 and $x$ = 0.1 respectively for one and three cycles of this iodine treatment. Compared to the minimal occupation reached by Kume et al[34], the Na removal rate reported here seems

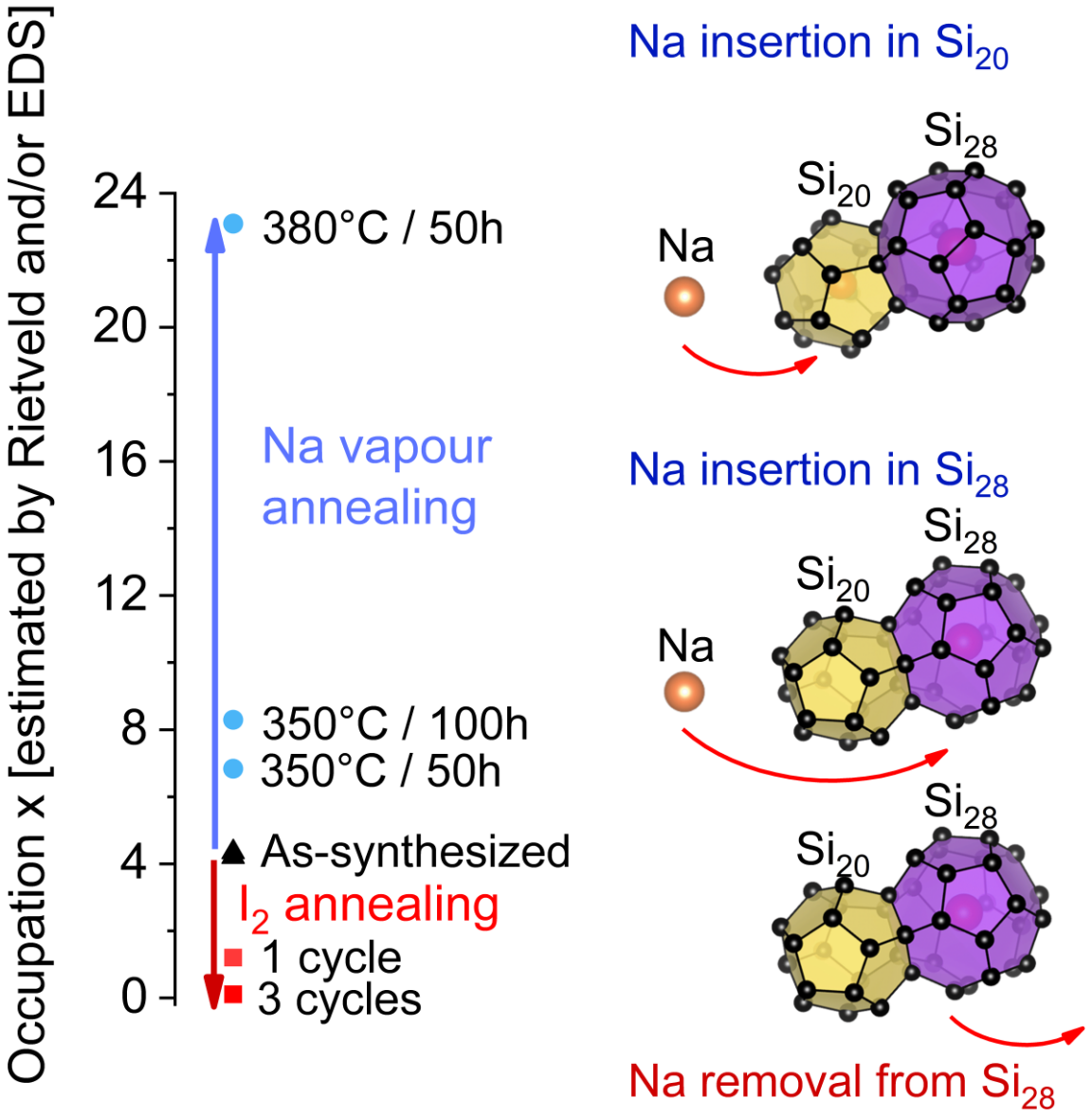


*FIG. 3. Effect on the sodium occupation of the SiCL-II of the annealing under iodine atmosphere in red and of the sodium vapour annealing in green.*

less efficient which could be due to the lower temperature of annealing which is limited by the custom setup. Nonetheless, this process allows the obtention of Na occupation unattainable using only the annealing under vacuum method. For comparison purpose, Figure 1b exhibits diffractograms of the almost guest-free, routinely synthesized and fully occupied structures next to each other while Figure 3 sums up the range of occupations accessible taking advantage of the various process. SiCL-I films were also submitted to these treatments without change in their composition without surprise.

Hall effect measurements were performed to determine the impact of the occupation on the electrical properties of our samples with thickness around 30 µm. The results

are listed in Table I for SiCL-I sample but also SiCL-II sample from almost guest free to *x* = 23. The SiCL-I film exhibits metallic behavior with 4.3 x $10^{-2}$ Ω·cm and carrier mobility of 43 cm²/(V·s) as expected. For SiCL-II, there is a 4 order of magnitude variation of resistivity depending on the amount of Na located in the cages of the structure. The evolution of the electrical resistivity is rising as the Na atoms are evacuated from the Silicon Clathrates cages. This evolution seems to drastically quicken when coming close either to the guest free $Si_{136}$ structure or to the completely filled $Na_{24}Si_{136}$. The SiCL-II films as-synthesized (x = 6 to 2) are direct band-gap n-type semiconductors as shown in our previous work[24], which can be turned into the metallic phase $Na_{24}Si_{136}$ exhibiting a resistivity close to its SiCL-I counterpart or to the $Si_{136}$, which would truthfully be an allotrope of Silicon. No major variation in terms of carrier mobility is observed as *x* is changing, there is a slight rise for samples with low occupation while it seems to be reduced when the small cages are starting to be filled and that the phase is becoming more and more metallic. The amplitude of the variation of the resistivity is similar to measurement single crystals[26].

*TABLE I. Electrical properties of the Silicon Clathrates as synthesized and submitted to various post-synthesis treatment.*

| Type of SiCL | Treatment undergone | Formula | Carrier concentration ($cm^{-3}$) | Resistivity (Ω·cm) | Mobility ($cm^2/(V·s)$) |
|---|---|---|---|---|---|
| **SiCL-I** | *As-synthesized* | $Na_8Si_{46}$ | -1.5 x $10^{19}$ | 4.3 x $10^{-2}$ | 43 |
| **SiCL-II** | *3 Cycles of $I_2$ annealing* | $Na_{\sim 0.1}Si_{136}$ | -3.6 x $10^{16}$ | 110 | 15 |
| | *1 Cycle of $I_2$ annealing* | $Na_1Si_{136}$ | -9.2 x $10^{16}$ | 40.7 | 21 |
| | *As-synthesized* | $Na_{4.2}Si_{136}$ | -2.1 x $10^{17}$ | 4.2 | 7.1 |
| | | $Na_{4.35}Si_{136}$ | -3.0 x $10^{17}$ | 2.2 | 8.0 |
| | *Na vapor 350°C for 50h* | $Na_{6.9}Si_{136}$ | -9.2 x $10^{17}$ | 6.3 x $10^{-1}$ | 13.3 |
| | *Na vapor 350°C for 50+50h* | $Na_8Si_{136}$ | -6.5 x $10^{18}$ | 3.3 x $10^{-1}$ | 6.1 |
| | *Na vapor 380 for 50H* | $Na_{23}Si_{136}$ | -5.4 x $10^{20}$ | 1.1 x $10^{-2}$ | 4.1 |

However, their resistivities remain lower than the ones reported for powders samples hot-pressed into pellet[35] with close to two orders of magnitude factor and are higher than the value reported for single crystals by three orders of magnitude[26]. This difference is most likely due to the presence of numerous defaults and cracks in the Silicon Clathrates films[19,22,23] usually obtained by the thermal decomposition process which makes it even harder for charge carriers to move through the material. This gradual shift from a rather insulating phase to a metallic phase is due to the more and more intense hybridization between the Na atoms and the silicon framework conductivity as the $Si_{20}$ cages are being filled.

Raman Spectroscopy is also used to inspect the above-mentioned samples and shown in Figure 4. Most of samples show good peak definition for all wavenumber investigated except for the SiCL-I sample and the SiCL-II for occupation above $x = 8$ as it can be seen from the lower signal to noise ratio compared to the other samples. From the previous electrical measurements, it is obvious that this low signal harvesting for these samples is due to their metallic character lowering the effectiveness of the change in polarizability during molecular vibration on which rely Raman spectroscopy. For all samples, no characteristic peaks of amorphous or crystalline silicon are observed. The SiCL-I exhibit predominantly a $T_{2g}$ vibration at 169 $cm^{-1}$ with two other $T_{2g}$ vibrations at 114 and 125 $cm^{-1}$ and a $E_g$ one at 135 $cm^{-1}$, while the other peaks are not enough defined to differentiate them. Those values are close to the Raman active vibrational mode calculated for $Si_{46}$[36,37] with a slight low frequency shift for the $E_g$ mode and high frequency shift for the $T_{2g}$. For the SiCL-II samples, gradual shifts of the raman peaks are observed as the occupation is changed and depict for more

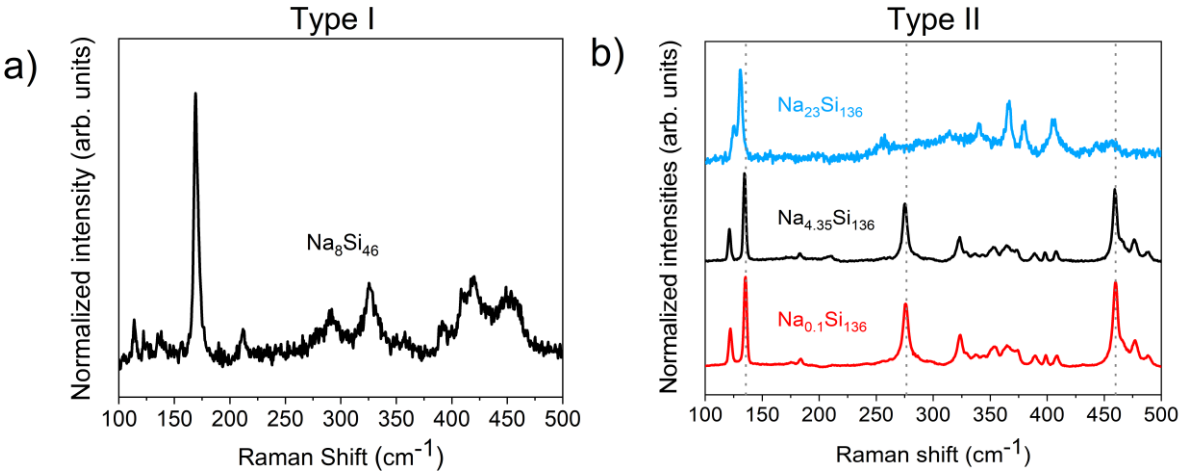


*FIG. 4. Raman spectra for a) SiCL-I b) SiCL-II with low, classic and high sodium occupation.*

occupation values in Figure S6. For low occupation, the peaks are well defined and as *x* is increased, all the peaks are subject to a low frequency shift. This shift is subtle and is observed for all the peaks. As *x* is superior to 8 and thus when the small cages are partially or almost completely filled, the Raman vibrations are of reduced intensities, and most of them are impossible to differentiate from each other's. Nonetheless, the peak energies are still subject to change. All identifiable peaks are keeping their movement toward lower frequencies this time, and as the small cages are being filled this shift is striking compared to lower occupation. The forementioned peaks and their corresponding wavenumber are listed in Table II. This red-shift phenomenon is often correlated with a crystallinity increase or when a material is subjected to tensile stress moving atoms away from each other. In our case, this shift is surely due to the expansion of the lattice parameters and thus of the chemical bonds' expansion, explaining the barely noticeable shift when the small cages are filled with lattice parameters revolving around 14.64 Å which become obvious when the structure is fully occupied and extend to 14.71 Å[33,38].

*Table II: Energies of the various Raman vibrations for the SiCL-II with low, classic, high sodium occupation compared to tabulated values.*

| Vibration mode | $Si_{136}$ theory by Nolas *et al.* ($cm^{-1}$)[39] | $Na_{0.1}Si_{136}$ ($cm^{-1}$) | $Na_{4.35}Si_{136}$ ($cm^{-1}$) | $Na_{23}Si_{136}$ ($cm^{-1}$) |
|---|---|---|---|---|
| $1T_{2g}$ | 121 | 122.7 | 121.6 | - |
| $1E_g$ | 130 | 135.9 | 134.9 | 131.6 |
| $2T_{2g}$ | 176 | 184.3 | 183.5 | - |
| $3T_{2g}$ | 267 | 276.7 | 275.7 | 257.0 |
| $1A_{1g}$ | 316 | 323.9 | 323.8 | 314.5 |
| $4T_{2g}$ | 325 | 330.7 | 330.2 | - |
| $2_{Eg}$ | 360 | 365.8 | 365.4 | 367.2 |
| $2A_{1g}$ | 397 | 398.2 | 398.4 | - |
| $5T_{2g}$ | 406 | 408.4 | 407.8 | 406.7 |
| $3A_{1g}$ | 458 | 461.1 | 460.6 | 442.5 |
| $3_{Eg}$ | 463 | Not resolved from $3A_{1g}$ | | 456.0 |
| $6T_{2g}$ | 466 | | | - |
| $7T_{2g}$ | 473 | 477.2 | 477.1 | - |
| $8T_{2g}$ | 487 | 489.4 | 488.4 | - |

Figure S7 displays the photoluminescence spectra of various Silicon Clathrates films of various Na concentration. The broad peaks obtained are similar to previous results[22,24,40], centered at 1.65 eV and 1.70 eV for $Na_{0.1}Si_{136}$ and $Na_{4.35}Si_{136}$ respectively with a possible contribution of less intense peak located at 1.8 eV originating from a surfacing disordered silicon materials as reported previously[22]. For $Na_{23}Si_{136}$, as the phase is metallic no peak is observed except the one related to surfacing impurities.

Transport measurements are performed on two different SiCL-II samples: highly occupied samples with $x$ = 23 and the almost guest free $Na_{0.1}Si_{136}$. Figure 5 shows the temperature dependence of the measured sheet resistance which behavior is modulated from the metallic $Na_{23}Si_{136}$ to the semiconducting $Na_{0.1}Si_{136}$. This variation characterize also powder[41] and single-crystal[12] samples. The increase of the resistivity with the decrease of the Na occupation originates from the more and more isolated state of the Na cluster further limiting the electron hoping at low temperature as revealed by Electron Spin Resonance measurements[42].

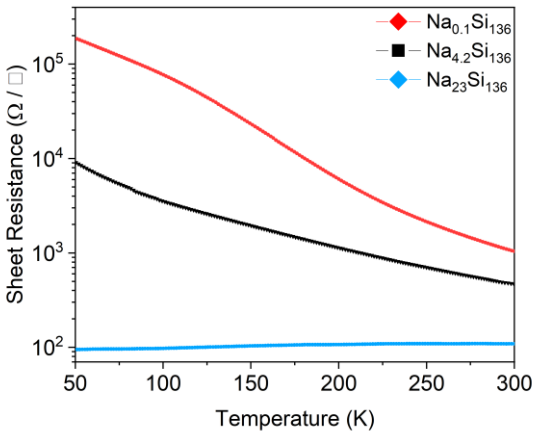


*FIG. 5. Sheet Resistance versus temperature measurements for the SiCL-II different cages occupations.*

DFT calculations of the densities of states for several SiCL-I and SiCL-II structures are reported in Figure 6. For the type I, both the experimentally obtained fully occupied structure and the guest-free $Si_{46}$ densities of states were calculated. The guest-free

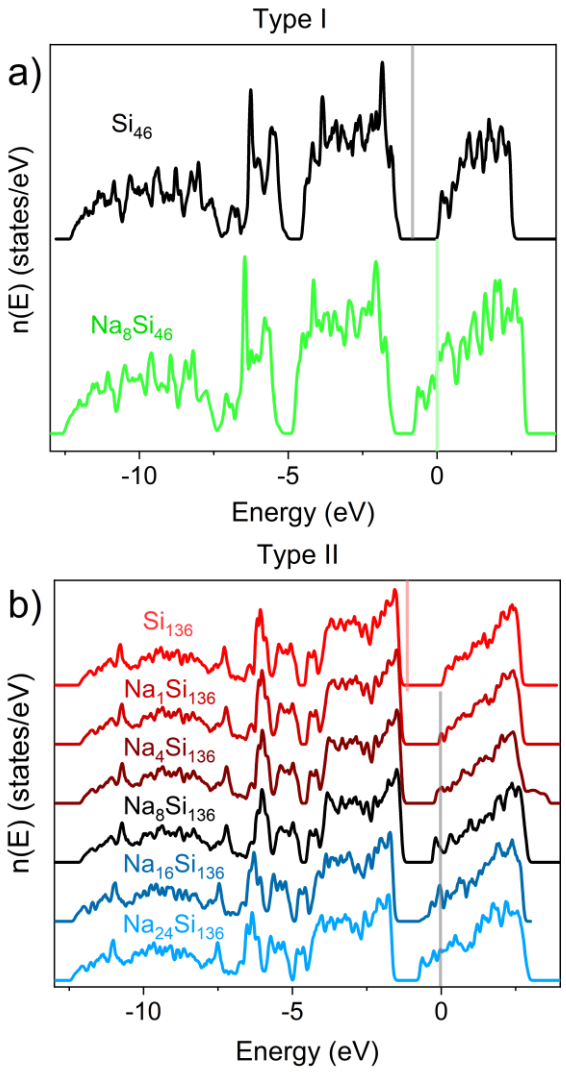


*FIG. 6. Total Density of States calculated by DFT for a) Guest free and fully occupied SiCL-I b) Guest free and various occupation values of SiCL-II. The Fermi level corresponds to the vertical bar and is set to the energy origin for Na occupied SiCL.*

SiCL-I exhibits a bandgap of 1.13 eV with a top-valence band originating from p states of the silicon while the bottom is due almost exclusively to the s states while the conduction band is originating both from p states and a non-negligible s states contribution. When the eight cages of the structure are filled with Na atoms, the valence band shows no significant change in its content while the conduction band is gathering both the previous Silicon contribution but also s states from the Na atoms. This Na contribution induces the extension of the conduction band by the hybridization between the silicon framework states and the states of the Na guests similarly observed in literature[43,44]. Thus, the Fermi level is now located in the conduction band, indicating a metallic behavior while the energy-gap between the two band is reduced to 0.53 eV. The two $Si_{136}$ and $Si_{46}$ calculated structures exhibits quite similar density of states due

to their relatively close structures, exhibiting a 1.19 and a 1.13 eV gap respectively. The valence band of SiCL-II structure is due to the same silicon states than the SiCL-I one. Similarly, the gradual filling of the cages by the Na atoms induces an extension of the conduction band thanks to the hybridization of the Na states with the states of the silicon framework. For the SiCL-II structure, TDOS has been calculated following a gradual filling of the structure, in a likewise fashion than Xue *et al.* study[45], starting by the 8 $Si_{28}$ cages until they are all full to then fill the 16 $Si_{20}$ cages. As soon as a Na atom is inserted into the structure, the hybridization causes the Fermi level to be located at the edge of the conduction band and the reduction of the gap between the bands. The “closure” of the gap is happening steadily as the occupation is increased to reach a maximum at the fully occupied structure where the gap is only of 0.59 eV with a Fermi level located inside of the conduction band.

The DFT calculations of the two structures with different Na occupation indicate the transition from a semiconducting guest-free materials toward a metallic fully occupied material as Na content is increased. Calculated band structures for $x$ = 0, 1 and 8, visible on Figure S8, highlight this gradual closure of the gap between the band while indicating a change of its nature from direct to slightly indirect. These results are in agreement with the previous electrical measurements at room temperature and versus temperature.

**V. Conclusion**

Obtention pathways of Type-II Silicon Clathrate film with composition ranging from almost guest-free to fully occupied are reported. Modification of the synthesis method is not sufficient to obtain neither low nor high occupancy, to reach them, post-synthesis annealing in iodine atmosphere or exposition to Na vapour are crucial. As the occupation is increased, Type-II Silicon Clathrates exhibit a stronger metallic character due to the shorten distance between Na atoms and their high hybridization with the silicon framework. Conversely, when the Na content is decreased, the Na clusters are isolated from each other preventing the electrons movements thus reducing the conductivity of the semiconductive phase with a bandgap around 1.7-1.9 eV. Resistance versus temperature measurements of the Silicon Clathrates films are

reported for the first time, and further assess the impact of low Na concentration on the electrical properties of the material. Total density of states and band structures obtained by DFT highlight the insulator to metal transition by the growing Na hybridization with the silicon framework as the cages are filled.

These DFT calculations indicate a similar transition for the SiCL-I impelling innovative new synthesis or guest-removal methods to attain them. Guest-free $Si_{46}$ would be a material of interest just like the SiCL-II Clathrates, allowing to obtain films whose behavior can be easily changed from metallic to semiconductive, with tunable resistivities.

**Supplementary Material**

See the supplementary material for additional information about the setup used for the iodine cycling, the values of the parameters obtained by Rietveld refinement of the various film along with EDS measurements backing their refined Na concentration. Supplementary Raman spectra for more occupation's values are available along with PL measurements and the band structures obtained by DFT.

**Acknowledgments**

We would like to thank Nicolas Zimmerman and Jeremy Bartringer for technical assistance, along with Marc Lenertz and the XRD platform of the IPCMS. This project has received financial support from the CNRS through the 80|Prime program. The authors would like to acknowledge the High Performance Computing Center of the University of Strasbourg for supporting this work by providing access to computing resources. Part of the computing resources were funded by the Equipex Equip@Meso project (Programme Investissements d'Avenir) and the CPER Alsacalcul/Big Data.

**Conflict of Interest**

The authors have no conflicts to disclose.

## Author Contributions

**R. Vollondat:** Conceptualization (equal), Investigation (lead), Methodology (equal), Writing – original draft (lead). **D. Stoeffler:** Investigation (supporting), Writing – review & editing (supporting), Methodology (equal). **D. Preziosi:** Investigation (supporting), Writing – review & editing (supporting). **S. Roques:** Investigation (supporting). **A. Slaoui:** Conceptualization (equal), Project Administration (supporting). **T. Fix:** Conceptualization (equal), Project Administration (lead), Writing – review & editing (lead).

## Data availability

The data that support the findings of this study are available within the article and its supplementary material and are available from the corresponding author upon reasonable request.

## References


1 H. Davy, *Philos. Trans. R. Soc. Lond.*, 1811, **101**, 155–162.
2 E. Reny, S. Yamanaka, C. Cros and M. Pouchard, *J. Phys. Condens. Matter*, 2002, **14**, 11233–11236.
3 K. Wei, Y. Dong and G. S. Nolas, *J. Solid State Chem.*, 2016, **237**, 81–85.
4 F. Sui and S. M. Kauzlarich, *Chem. Mater.*, 2016, **28**, 3099–3107.
5 Y. Zhang, J. Brorsson, R. Qiu and A. E. C. Palmqvist, *Adv. Electron. Mater.*, 2021, **7**, 2000782.
6 H. Kawaji, H. Horie, S. Yamanaka and M. Ishikawa, *Phys. Rev. Lett.*, 1995, **74**, 1427–1429.
7 A. Martinez, L. Krishna, L. Baranowski, M. Lusk, E. Toberer and A. Tamboli, *Photovolt. IEEE J. Of*, 2013, **3**, 1305–1310.
8 P. Warrier and C. A. Koh, *Appl. Phys. Rev.*, 2016, **3**, 040805.
9 K. S. Chan, M. A. Miller and X. Peng, *Mater. Res. Lett.*, 2018, **6**, 72–78.
10 J. S. Kasper, P. Hagenmuller, M. Pouchard and C. Cros, *Science*, 1965, **150**, 1713–1714.
11 E. Reny, M. Ménétrier, C. Cros, M. Pouchard and J. Sénégas, *Comptes Rendus Académie Sci. - Ser. IIC - Chem.*, 1998, **1**, 129–136.
12 S. Iwasaki, H. Morito, T. Komine, K. Morita, T. Shibuya, J. Nishii and M. Fujioka, *Adv. Mater.*, 2022, **34**, 2106754.
13 A. Ammar, C. Cros, M. Pouchard, N. Jaussaud, J.-M. Bassat, G. Villeneuve and E. Reny, *J. Phys. IV Proc.*, 2005, **123**, 29–34.
14 A. M. Guloy, R. Ramlau, Z. Tang, W. Schnelle, M. Baitinger and Y. Grin, *Nature*, 2006, **443**, 320–323.
15 S. Yamanaka, M. Komatsu, M. Tanaka, H. Sawa and K. Inumaru, *J. Am. Chem. Soc.*, 2014, **136**, 7717–7725.

16 M. Beekman, A. J. Karttunen, W. Wong-Ng, M. Zhang, Y.-S. Chen, C. Posadas, A. Jarymowycz, E. Cruse, W. Peng, A. Zevalkink, J. A. Kaduk and G. S. Nolas, *Phys. Rev. B*, 2022, **105**, 214114.
17 X. Blase, *Phys. Rev. B*, 2003, **67**, 035211.
18 H. Horie, T. Kikudome, K. Teramura and S. Yamanaka, *J. Solid State Chem.*, 2009, **182**, 129–135.
19 F. Ohashi, Y. Iwai, A. Noguchi, T. Sugiyama, M. Hattori, T. Ogura, R. Himeno, T. Kume, T. Ban and S. Nonomura, *J. Phys. Chem. Solids*, 2014, **75**, 518–522.
20 United States, US6103403A, 2000.
21 R. Kumar, Y. Hazama, F. Ohashi, H. S. Jha and T. Kume, *Thin Solid Films*, 2021, **734**, 138859.
22 Y. Liu, W. K. Schenken, L. Krishna, A. A. A. Majid, T. E. Furtak, M. Walker, C. A. Koh, P. C. Taylor and R. T. Collins, *Appl. Phys. Rev.*, 2021, **8**, 041408.
23 T. Fix, R. Vollondat, A. Ameur, S. Roques, J.-L. Rehspringer, C. Chevalier, D. Muller and A. Slaoui, *J. Phys. Chem. C*, 2020, **124**, 14972–14977.
24 R. Vollondat, S. Roques, C. Chevalier, J. Bartringer, J.-L. Rehspringer, A. Slaoui and T. Fix, *J. Alloys Compd.*, 2022, **903**, 163967.
25 V. Petříček, M. Dušek and L. Palatinus, *Z. Für Krist. - Cryst. Mater.*, 2014, **229**, 345–352.
26 S. Stefanoski, C. D. Malliakas, M. G. Kanatzidis and G. S. Nolas, *Inorg. Chem.*, 2012, **51**, 8686–8692.
27 G. Kresse and J. Furthmüller, *Phys. Rev. B*, 1996, **54**, 11169–11186.
28 G. Kresse and D. Joubert, *Phys. Rev. B*, 1999, **59**, 1758–1775.
29 P. E. Blöchl, *Phys. Rev. B*, 1994, **50**, 17953–17979.
30 J. P. Perdew, K. Burke and M. Ernzerhof, *Phys. Rev. Lett.*, 1996, **77**, 3865–3868.
31 K. S. Chan, M. A. Miller, W. Liang, C. Ellis-Terrell and C. K. Chan, *J. Mater. Res.*, 2016, **31**, 3657–3665.
32 K. Momma and F. Izumi, *J. Appl. Crystallogr.*, 2011, **44**, 1272–1276.
33 M. Beekman, E. N. Nenghabi, K. Biswas, C. W. Myles, M. Baitinger, Y. Grin and G. S. Nolas, *Inorg. Chem.*, 2010, **49**, 5338–5340.
34 T. Kume, F. Ohashi, K. Sakai, A. Fukuyama, M. Imai, H. Udono, T. Ban, H. Habuchi, H. Suzuki, T. Ikari, S. Sasaki and S. Nonomura, *Thin Solid Films*, , DOI:10.1016/j.tsf.2016.03.056.
35 M. Beekman and G. S. Nolas, *Phys. B Condens. Matter*, 2006, **383**, 111–114.
36 M. Menon, E. Richter and K. R. Subbaswamy, *Phys. Rev. B*, 1997, **56**, 12290–12295.
37 D. Kahn and J. Ping Lu, *Phys. Rev. B*, 1997, **56**, 13898–13901.
38 T. Ban, T. Ogura, Y. Ohashi, R. Himeno, F. Ohashi, T. Kume, Y. Ohya, H. Natsuhara, T. Iida, H. Habuchi and S. Nonomura, *J. Mater. Sci.*, 2013, **48**, 989–996.
39 G. S. Nolas, C. A. Kendziora, J. Gryko, J. Dong, C. W. Myles, A. Poddar and O. F. Sankey, *J. Appl. Phys.*, 2002, **92**, 7225–7230.
40 L. Krishna, A. D. Martinez, L. L. Baranowski, N. P. Brawand, C. A. Koh, V. Stevanović, M. T. Lusk, E. S. Toberer and A. C. Tamboli, in *Physics, Simulation, and Photonic Engineering of Photovoltaic Devices III*, SPIE, 2014, vol. 8981, pp. 29–39.
41 C. Cros, M. Pouchard and P. Hagenmuller, *J. Solid State Chem.*, 1970, **2**, 570–581.
42 M. Yamaga, T. Kishita, K. Goto, S. Sunaba, T. Kume, T. Ban, R. Himeno, F. Ohashi and S. Nonomura, *J. Phys. Chem. Solids*, 2020, **140**, 109358.
43 W. Zhang, Q.-Y. Chen, Z.-Y. Zeng and L.-C. Cai, *Chin. Phys. B*, 2015, **24**, 107101.
44 J. C. Conesa, C. Tablero and P. Wahnón, *J. Chem. Phys.*, 2004, **120**, 6142–6151.

45 D. Xue and C. Myles, *Materials*, 2019, **12**, 536.